Science of the Total Environment 647 (2019) 88–98

Contents lists available at ScienceDirect

Science of the Total Environment

journal homepage: www.elsevier.com/locate/scitotenv

Extrinsically magnetic poly(butylene succinate): An up-and-coming petroleum cleanup tool

André Segadas Figueiredo [a], Luis Peña Icart [b], Fernanda Davi Marques [c], Edson Rodrigo Fernandes [a], Letícia Pedretti Ferreira [c], Geiza Esperandio Oliveira [a,d], Fernando Gomes Souza Jr. [a,c,*]

[a] Programa de Engenharia Civil, COPPE, Centro de Tecnologia - Cidade Universitária, Av. Horácio Macedo, 2030, bloco I., Universidade Federal de Rio de Janeiro, 21941-450, Brazil
[b] Faculdade de Farmácia, Cidade Universitária, Av. Carlos Chagas Filho, 373, Universidade Federal de Rio de Janeiro, 21941-170, Brazil
[c] Instituto de Macromoléculas Professora Eloisa Mano, Centro de Tecnologia-Cidade Universitária, av. Horacio Macedo, 2030, bloco J., Universidade Federal de Rio de Janeiro, 21941-598, Brazil
[d] Programa de Engenharia Química, Centro de Tecnologia-Cidade Universitária, av. Horacio Macedo, 2030, bloco G., Universidade Federal de Rio de Janeiro, 21941-450, Brazil

HIGHLIGHTS

- This paper deals with the control of petroleum spilled out.
- The synthesis and characterization of extrinsically magnetic PBS is presented.
- The best material can remove 11 g of oil per gram of composite.
- The best material is a better choice than peat.
- Aliphatic/aromatic balance is the key to a higher oil sorption capability.

GRAPHICAL ABSTRACT

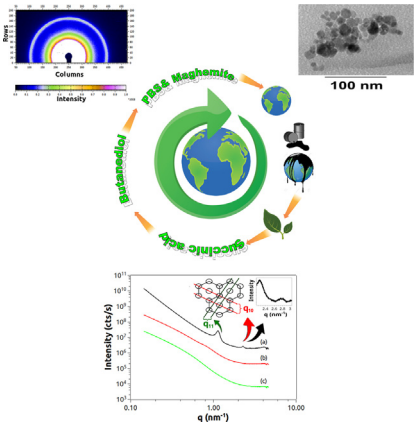

ARTICLE INFO

Article history:
Received 16 February 2018
Received in revised form 11 June 2018
Accepted 30 July 2018
Available online 31 July 2018

Editor: Baoliang Chen

Keywords:
Poly(butylene succinate)
Maghemite
Magnetic composites
Petroleum
Oil spill cleanup

ABSTRACT

This work presents the synthesis and characterization of extrinsically magnetic poly(butylene succinate) (PBS). PBS is obtained from succinic acid (SA), which can be efficiently produced from renewable biomass by fermentation. Thus, the use of SA helps to remove CO_2 from the atmosphere, constituting a good way to accumulate carbon credits. The magnetic PBS here presented was prepared by fusion using different amounts of maghemite. Obtained materials were characterized using Fourier transform infrared spectroscopy (FTIR), Thermogravimetric analysis (TGA), Differential scanning calorimetry (DSC), X-ray diffraction (XRD), Small angle X-ray scattering and magnetic force tests. Besides, the oil removal capability (OR) of the samples was also studied. All the magnetic composites were able to remove petroleum from the water. Among them, the one filled with the highest amount of magnetic particles was able to remove 11 g of oil per gram of composite. Also, XRD and SAXS results showed that PBS is a long size oriented material, which allows it to work as a thermoset, avoiding its dissolution in organic contaminant medium. As PBS can also be considered as a platform, these are promising results for the oil spill cleanup applications.

* Corresponding author at: Instituto de Macromoléculas Professora Eloisa Mano, Centro de Tecnologia-Cidade Universitária, av. Horacio Macedo, 2030, bloco J., Universidade Federal de Rio de Janeiro, 21941-598, Brazil.
E-mail address: fgsj@ufrj.br (F.G. Souza).

https://doi.org/10.1016/j.scitotenv.2018.07.421
0048-9697/

1. Introduction

The oil extraction has been widening over the years. For instance, according to the U.S. Energy Information Administration (accessed in February 2018) during 2006 were produced 85.198 k barrels per day and during 2016 the number increased to 97.023 k barrels per day (U.S. Energy Information Administration, 2018). Due to the evolution of technology the exploration of this resource is mainly offshore. The impact of accidents increases in this scenario and the tendency is getting even higher in the future (A repeated sampling method for oil spill impact uncertainty and interpolation, 2017; Carroll et al., 2018; Clancy et al., 2018; Motta et al., 2018). Among them, the most noticed were: Amoco Cadiz, 1978 (Brittany, France - 68.7 million of gallons); Ixtoc 1 Oil Well, 1979 (Bay of Campeche, Mexico - 140 million of gallons); Atlantic Empress, 1979 (Trinidad and Tobago, West Indies - 88.3 million of gallons); Nowruz Oil Field, 1983 (Persian Gulf - 80 million of gallons); Castillo de Bellver, 1983 (Saldanha Bay, South Africa - 78.5 million of gallons); Odyssey Oil Spill, 1988 (Nova Scotia, Canada - 43 million of gallons); M/T Haven Tanker, 1991 (Genova, Italy - 42 million of gallons); ABT Summer, 1991 (Coast of Angola - 80 million of gallons); Gulf War, 1991 (Kuwait - up to 336 million of gallons); Fergana Valley, 1992 (Uzbekistan - 87.7 million of gallons); and Deepwater Horizon, 2010 (Gulf of Mexico - 30 million of gallon) (Duan et al., 2018; Kaiser and Liu, 2018; Messina et al., 2016; Murphy et al., 2016; Rabalais et al., 2018; Wise et al., 2018).

Ismail and Karim (2013) listed 66 disasters evolving tanks, and they concluded that, between 1964 and 2011, around 4270 K MT of petroleum were spilled worldwide. The damage to the environment is immeasurable since so many toxic substances in the sea increases and increases, producing severe damages to fauna and flora (Giari et al., 2012; Gunster et al., 1993; Heibati et al., 2017). Besides, some of the cleanup techniques, such as the use of dispersants, create mutations in wildlife (Medeiros et al., 2017). Beyond the environmental impacts, there were many economic losses, mainly suffered by the fishing and tourism industries. Thus, there is a global concern about the oil spill issue, and new technologies and materials are always researched.

Ordinarily, petroleum is sorbed using peat, a conventional raw material. One gram of this material can sorb around 4 g of oil when exposed to this medium for 5 min (Klavins et al., 2012). Among the new technologies, the use of polymer systems is widely researched, and several studies reported these systems as oil spill cleanup tools (Adebajo et al., 2003; Ferreira et al., 2012; Grance et al., 2012; Reynolds et al., 2001; Li et al., 2012; Lin et al., 2012; Marques et al., 2016; Varela et al., 2013; Wang et al., 2013; Zhu et al., 2011).

In this context, the use of magnetic nanocomposites based on biopolymers (Doshi et al., 2018a, 2018b; Lobakova et al., 2016; Wilton et al., 2018) can improve the efficiency of the cleanup process since these composites can be easily removed from the water by the utilization of a magnetic field (Avila et al., 2014; Gu et al., 2014; Raj and Joy, 2015; Su et al., 2017; Wang et al., 2016). For instance, our group produced a magnetic PU based on castor oil, toluene diisocyanate, and water by a bulk polymerization (Lopes et al., 2010). One gram of this material was able to remove 4 g of petroleum from the water. In other work, we prepared a magnetic resin based on lignin from Kraft process (Grance et al., 2012). One gram of this material was able to remove 11 g of oil from water. In turn, 1 g of our cardanol-furfuraldehyde/maghemite magnetic composites was able to remove 10 g of petroleum from the water (Varela et al., 2013). A similar material filled with acetylated curaua fibers was able to remove 12 parts of oil per gram of the composite from water (Varela et al., 2013). In our last work, we prepared an aliphatic/aromatic polyester matrix filled with coffee ground powder and maghemite (Marques et al., 2016). One gram of this material was able to remove 25 g of the petroleum from the water. Therefore, the use of polyesters is promising.

Among green polymers, the poly(butylene succinate) (PBS) is obtained by the polycondensation of 1,4-butanediol and succinic acid (Bourmaud et al., 2015; Charlier et al., 2015; Ferreira et al., 2017; Frollini et al., 2013; Li et al., 2014; Luzi et al., 2016; Nerantzaki et al., 2015; Phua et al., 2013). PBS is an aliphatic, thermoplastic and crystalline polyester with excellent thermal and mechanical properties (Di Lorenzo et al., 2017; Gigli et al., 2016). Also, due to new biotechnological routes used to the preparation of the succinic acid, this polymer is considered as a future platform material (Cheng et al., 2012; Xu and Guo, 2010). Nowadays, succinic acid can be efficiently produced from renewable biomass, such as crop stalks wastes, by batch fermentation (Li et al., 2010) helping to remove CO_2 from the atmosphere (Nghiem et al., 2010). Thus, besides succinic acid is becoming cheaper, the use of this chemical can be a profitable way to accumulate carbon credits. Furthermore, to the best of our knowledge, PBS was never used as an oil spill cleanup tool. Therefore, the primary objective of this work is the synthesis, characterization of PBS/maghemite nanocomposites and the use of these materials as a petroleum cleanup tool. In the best case, each gram of the magnetic material was able to remove 11 g of the oil. This amount of removed oil is a promising result for the oil spill cleanup applications.

2. Experimental

2.1. Materials

Poly(1,4-butylene succinate), Lot#MKBX5346V; hydrochloric acid (HCl); ferric chloride ($FeCl_3$); anhydrous sodium sulfite (Na_2SO_3); potassium hydroxide (KOH) and polyvinyl alcohol were purchased from Sigma-Aldrich at analytical grade. Petroleum [density: 0.9697 g/cm^3; API (@60 °F): 13.39; viscosity 6994 mPa·s] was kindly donated by PETROBRAS.

2.2. Synthesis of maghemite

As described in previous works (da Costa and Souza Jr., 2014; Grance et al., 2012; Lopes et al., 2010; Neves et al., 2011; Oliveira et al., 2013; Pereira et al., 2014, 2013; Souza et al., 2013; Souza Jr. et al., 2010a, 2010b; Varela et al., 2013), our group is using similar approaches to obtain this nanomaterial. Specifically, in the present work, aqueous solutions of hydrochloric acid (2 M), ferric chloride (2 M), and sodium sulfite (1 M) were prepared. Into a beaker, under continuous agitation, 30 mL of the ferric chloride solution and 30 mL of deionized water were added. Soon afterward, 20 mL of the sodium sulfite solution was added to the beaker, still under continuous agitation. The reaction product was precipitated by slowly adding 51 mL of concentrated ammonium hydroxide into the beaker under constant stirring. The medium was poured after 30 min. The obtained nanoparticles were washed several times using distilled water and finally dried to constant weight at 60 °C in an oven. After that, the sample was heating at 250 °C for 1 h.

2.3. Preparation of the composites

The following amounts of poly(butylene succinate) were weighed: 995, 985, 975, 965 and 950 mg. Then these samples were melted separately at 150 °C. Soon afterward this process, the following amounts of maghemite were mixed to the PBS: 5, 15, 25, 35 and 50 mg, respectively. These mixtures were prepared under mechanical stirring, which was kept until the obtaining of homogeneous material. The composites were cooled at room temperature, milled and then classified using a 400 Mesh sieve.

2.4. Characterization of the materials

Polymer, maghemite, and composites were analyzed using the following techniques.

2.4.1. Fourier transform infrared

Fourier transform infrared materials were studied using a Varian model 3100 FTIR Excalibur Series spectrophotometer (Japan). Samples were macerated with potassium bromide (1 mg/100 mg samples/KBr). Then, the FTIR spectra of the samples were recorded at room temperature, using a resolution of 4 cm^{-1}. Composites were also compared to pure PBS by the root mean squared error (RMSE), as we reported elsewhere (Ferreira et al., 2012). RMSE is very useful to study the misfit between experimental data and model (Kelley and Lai, 2011). Therefore, RMSE was calculated through linear regressions between transmittances of the composites and PBS, using the *least squares* approach. The transmittances were normalized from 1 to 100. The statistical analysis considered the significance level $(1 - p)$ of 95%. The p value is here the "statistical insignificance" of the result so that lower p values indicate better results (Cohen and Cohen, 1983). Therefore, it was established that the result was significant when p was lower than 0.05 and these values are highlighted in red (Souza Jr. et al., 2006).

2.4.2. Differential scanning calorimetry

Differential scanning calorimetry materials were studied with the help of the TA Q1000 V9.9 build 303 Calorimeter. Briefly, 5 mg of the samples were heated and cooled at a rate of 10 °C/min from −80 to 200 °C under nitrogen flow. Values of glass transition (Tg), melting temperature (Tm) and the crystallization temperature on cooling (Tcc) were taken in a cooling run after the second heating run.

2.4.3. Thermogravimetric analyses

Thermogravimetric analyses were performed using a TA TGA Q500 Thermoanalyser. Measurements were carried out under nitrogen at a heating rate of 20 °C/min up to 700 °C with a gas flow rate of 20 mL/min.

2.4.4. Transmission electron microscopy

Samples were prepared for Transmission electron microscopy (TEM) by drying nanoparticles on a copper grid that is coated with a thin layer of carbon. Then they were examined under a transmission electron microscope (FEI-Tecnai Spirit 12).

2.4.5. X-ray diffraction

The analyses were performed at room temperature, using a multipurpose X-ray diffraction in diffractometer Ultima IV from Rigaku Inc., model Miniflex with a radiation source that presented a potential difference of 40 kV and an electric current of 20 mA. The equipment target was a copper plate that produces CuKα radiation with a wavelength of 0.154 nm. The scan was carried out at 2θ values from 10 to 70°, with a goniometer step of 0.05°/min. The crystallite size (Lc) was calculated using the Scherrer's equation (Eq. (1)) (Scherrer, 1918):

$$Lc = \frac{K\lambda}{\beta cos(\theta)} \quad (1)$$

In Eq. (1), Lc is the crystallite size, K is the shape factor (which here was considered equal to 1), λ is the wavelength, β is the half-width and θ is the angle. The crystalline degree (Xc) was estimated using the Ruland method (Eq. (2)) (Ruland, 1961):

$$Xc = \frac{Ac \times 100}{Ac + Aa} \quad (2)$$

In Eq. (2), Ac is the crystalline area, and Aa is the amorphous area.

2.4.6. Small angle X-ray scattering (SAXS)

SAXS measurements were performed with the beam line of the Brazilian Synchrotron Light Laboratory (LNLS, Brazil D11A-SAXS1-20160027). This beam line is equipped with an asymmetrically cut and bent silicon (111) monochromator (λ = 1.743A°), which yields a horizontally focused X-ray beam. A linear position sensitive X-ray detector (PSD) and a multichannel analyzer were used to determine the SAXS intensity I(q) as a function of the modulus of the scattering vector q = (4π) sin θ, 2θ is the scattering angle. All SAXS patterns were corrected for the parasitic scattering intensity produced by the collimating slits, for the nonconstant sensitivity of the PSD, for the time varying intensity of the direct synchrotron beam and differences in sample thickness. Thus, the SAXS intensity was determined for all samples in the same arbitrary units, so that they can be directly compared to each other. Since the incident beam cross-section at the detection plane is small, no mathematical deconvolution of the experimental SAXS function was needed. The distance between sample and detector was equal to 890.86 mm, allowing a q range between 0.15 and 4.64 nm^{-1}.

2.4.7. Magnetic force

Magnetic force tests were performed using a homemade experimental setup, described elsewhere (Souza et al., 2013). This setup is constituted by an analytical balance Shimadzu AY-220, a voltage source ICEL PS-4100, a digital multimeter ICEL MD-6450, a gaussmeter GlobalMag TLMP-Hall-02; a home-made sample holder and a home-made electromagnet device. System calibration was performed in the absence of magnetic material. Firstly, using the amperemeter and the gaussmeter, a current versus magnetic field calibration was performed. Soon afterward a current versus mass calibration was also performed. Obtained results were used to predict part of the presented error. Magnetic force tests were performed following the mass variation of the sample in the presence of the different magnetic field, produced by the electromagnet. Then, the apparent variation of mass of the sample in the presence of magnetic field was calculated subtracting the mass of the sample in the presence of magnetic field from the mass of the sample. The magnetic force (opposite to gravitational one) was calculated according to Eq. (3).

$$F_m = \Delta m \cdot g \quad (3)$$

where F_m is the magnetic force, Δm is the apparent variation of mass in the presence of the magnetic field and g is the acceleration of gravity. As a reference, the magnetic force of cobalt (II) chloride hexahydride standard sample was calculated according to this method, and the obtained result is equal to (0.11 ± 0.01) mN at (458 ± 3) G.

2.4.8. Crude oil magnetic removal

These tests were performed using synthetic brine, prepared using sodium chloride and calcium chloride as described elsewhere (Ferreira et al., 2012; Grance et al., 2012; Marques et al., 2016).

Gravimetric oil removal capability was evaluated following the next steps: Firstly the magnetic composite is weighed (w_1); then 90 ml of the brine is poured into a beaker and the total mass is determined; in next step a known mass of the oil (w_2) is spilt on the water; so the magnetic composite is added into the beaker (containing the water and the oil). After 5 min the oil and composite are magnetically removed using a Nd magneto (850 G); finally the mass of the oil residue is determined (w_3) and the gravimetric oil removal (Or) is calculated according to Eq. (4).

$$Or = \frac{w_2 - w_3}{w_1} \quad (4)$$

Weighing was carried out with the help of an analytical scale. The temperature was kept equal to 23 °C during the experiments.

3. Results

The magnetite synthesis procedure by homogeneous co-precipitation produced a dark colored material, which, after oxidation at 250 °C, shifts to a reddish one, named maghemite. Similar results

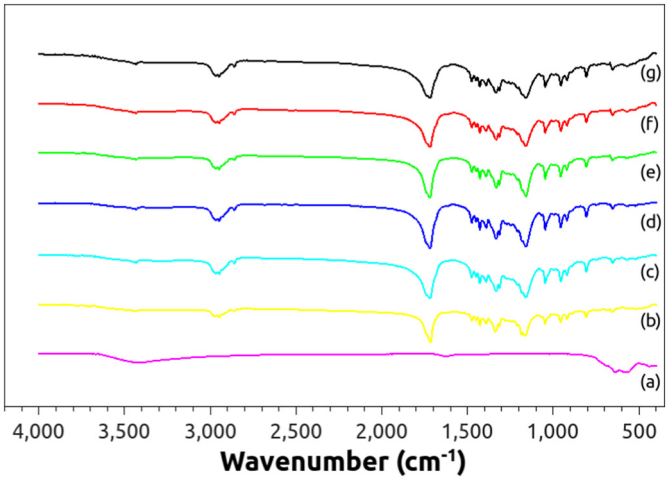

Fig. 1. FTIR of maghemite (a), PBS (b), and composites containing 0.5 (c), 2.5 (d) and 5.0% (e) of maghemite.

were found by other authors (Roca et al., 2007; Schwertmann and Cornell, 2008). Composites were prepared using different amounts of maghemite and the observed weight losses, with a confidence limit of 95%, were equal to 19 ± 11%.

Fig. 1 shows the FTIR spectra of maghemite, PBS, and composites. The maghemite spectrum shows the wide characteristic band at 3426 cm^{-1}, related to the stretching of O—H bond from FeOH. This band is wide due to the hydrogen bonds produced by the OH group. There is a characteristic band at 1641 cm^{-1} associated with the presence of structural water. The characteristic bands observed at 645 and 576 cm^{-1} are attributed to Fe—O bond from the ε-Fe_2O_3 and α-Fe_2O_3 stretching, respectively. These results are in agreement with others published elsewhere by our group (Oliveira et al., 2013; Souza et al., 2013; Souza Jr. et al., 2010a).

The PBS spectrum presents a smooth wide characteristic band around 3500 cm^{-1} associated with hydrogen bonds from some residual succinic acid. This result is corroborated by the presence of the small peak at 3449 cm^{-1}, which is attributed to C—H stretching from succinic acid (Kennouche et al., 2016). Also, other characteristic bands can be related to residual acid in the system, including those at 1428 and 921 cm^{-1}, corresponding the C—O—H and O—H groups asymmetric stretching in the acid molecule, respectively.

The main characteristic bands of PBS are the doublet at 2988 and 295 cm^{-1}, which is related to the C—H stretching. The stretching of the C═O bond appears as a strong and sharp peak at 1717 cm^{-1}. The characteristic bands at 1476 and 1451 cm^{-1} are associated with CH_3 symmetric and asymmetric deformation, respectively. The coupled deformation of C—C(C═O)—O group from ester shows up at 1315 and 958 cm^{-1}. The symmetric and asymmetric angular deformations of C—H bonds are seen at 1392 and 1340 cm^{-1}, respectively. The stretching of C—O—C group appears at 1186 cm^{-1}, while the stretching of —C—O—C— group in the ester linkages is observed at 1168 cm^{-1} (Kennouche et al., 2016; Silverstein et al., 2005). The (C═O)—O groups vibration are centered at 1049 cm^{-1}.

The composites spectra presented similar profile as that one to PBS, with the same characteristic bands. This fact indicates that the maghemite presence did not change the chemical nature of the PBS. It suggests that the fusion process used to the preparation of the composites caused no deterioration on the polymer. On the other hand, the maghemite was not directly detected in these samples. In spite very similar, obtained spectra presented differences. These differences can be expressed using the root mean squared error (RMSE). RMSE is very useful to study the misfit between experimental data and model (Kelley and Lai, 2011). Therefore, RMSE was calculated through linear regressions between transmittances of the PBS and composite, using the *least squares* approach. The obtained results are shown in Table 1. The R^2 between the used amount of maghemite and calculated RMSE is equal to 0.9738. This result proves that different amounts of maghemite are present in hybrid materials.

The PBS and the composites were also characterized by TGA and DSC. Key results are shown in Table 1.

TGA was used to establish the temperature where the maximum degradation rate (Tdeg) took place, while DSC was used to infer the influence of the magnetic nanoparticles on the matrix properties. The degradation temperature of the pure PBS was equal to 380.0 °C. In turn, the average Tdeg value of the composites was equal to (383.1 ± 0.3) °C, with a confidence level equal to 95%. Thus, even the lowest amount of maghemite was able to produce an increase of the thermal resistance of the PBS. Similar behavior was already reported to PLGA/maghemite composites (Silva et al., 2015).

Among the calorimetric results, the highest positive correlation, equal to 0.957551, was observed between the used amount of maghemite and the crystallization temperature. In turn, the obtained values of the melting temperature were not influenced by the maghemite, and the average Tm value was equal to (113.4 ± 0.2) °C, with a confidence level equal to 95%. Thus, even the lowest amount of maghemite was not able to produce changes in the structure of the crystals of the macromolecule. On the other hand, the highest negative correlation, equal to −0.954748, was observed between the used amount

Table 1
Main properties of the tested materials obtained from XRD, FTIR and TGA/DSC tests.

Analysis	Properties	Maghemite (wt%)						R[#]	p[#′]
		0.0	0.5	1.5	2.5	3.5	5.0		
XRD	Xc (%)[$]	51.5	54.0	51.4	47.9	44.5	42.3	−0.952	0.003
	Area[&]	1503.38	1063.30	936.50	793.74	647.07	506.61	−0.928	0.008
	Height[&]	2017.61	2219.79	1759.57	1491.33	1350.85	1057.62	−0.966	0.002
	FWHM[&]	0.70	0.45	0.50	0.50	0.45	0.45	−0.609	0.199
FTIR	R^2 [+]	1.0000	0.9713	0.9699	0.9595	0.9442	0.9332	−0.947	0.004
	RMSE[+]	0.0000	1.0879	2.2555	3.1193	5.1366	5.9651	0.987	0.001
TGA/DSC	Tdeg (°C)	380.0	382.9	383.4	383.3	383.0	383.0	0.534	0.257
	Tc (°C)	76.7	77.6	78.3	78.3	78.8	79.8	0.958	0.003
	Tm (°C)	113.2	113.4	113.3	113.4	113.4	113.6	0.850	0.032
	SCD (°C)[*]	36.5	35.8	35.0	35.1	34.6	33.8	−0.955	0.003
	tc (s)[*′]	109.5	107.4	105.0	105.3	103.8	101.4	−0.958	0.004

[$] Crystallinity degree obtained by XRD.
[&] Values calculated using peak centered @ 2θ = 22.64°.
[+] Coefficient of determination (R^2) and root mean squared error (RMSE) calculated by linear regressions between transmittances of the composites versus PBS.
[#] Correlation between properties values and the used amount of maghemite (statistically significant cases ($p < 0.05$) are in red).
[#′] Significance level.
[*] Supercooling degree.
[*′] Crystallization time from melting.

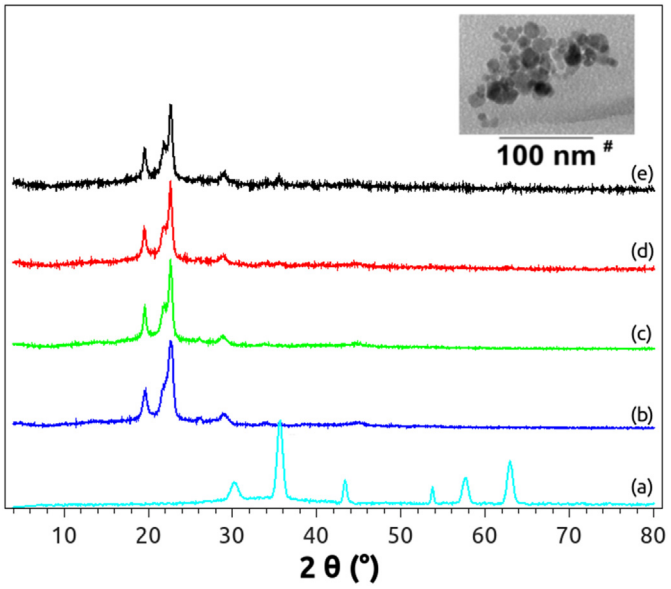

Fig. 2. XRD of maghemite (a), PBS (b) and composites containing 0.5 (c), 2.5 (d) and 5.0% (e) of maghemite. Inset (#) shows the TEM of the magnetic nanoparticles.

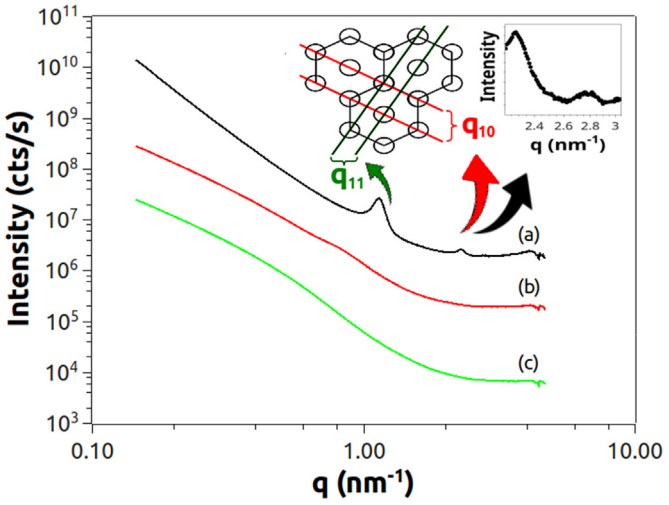

Fig. 4. One-dimensional SAXS patterns of PBS (a), a composite containing 5.0% of maghemite (b), and maghemite (c). The inset shows details of the planes q_{11}, and q_{10}, and SAXS region containing peaks q_{10}, and its harmonic q_{20}.

of maghemite and the Supercooling degree (SCD). Therefore, this result demonstrates that maghemite can reduce the SCD and the crystallization time (tc) of PBS. This reduction of the nucleation time results in a more efficient heating absorption or release along the melting and solidifying transformations, allowing a lower energy consumption to obtain these phase changes (Liu et al., 2015).

Fig. 2 presents the XRD diffraction pattern of the maghemite. Maghemite exhibits the following diffraction peaks, at 2θ values:

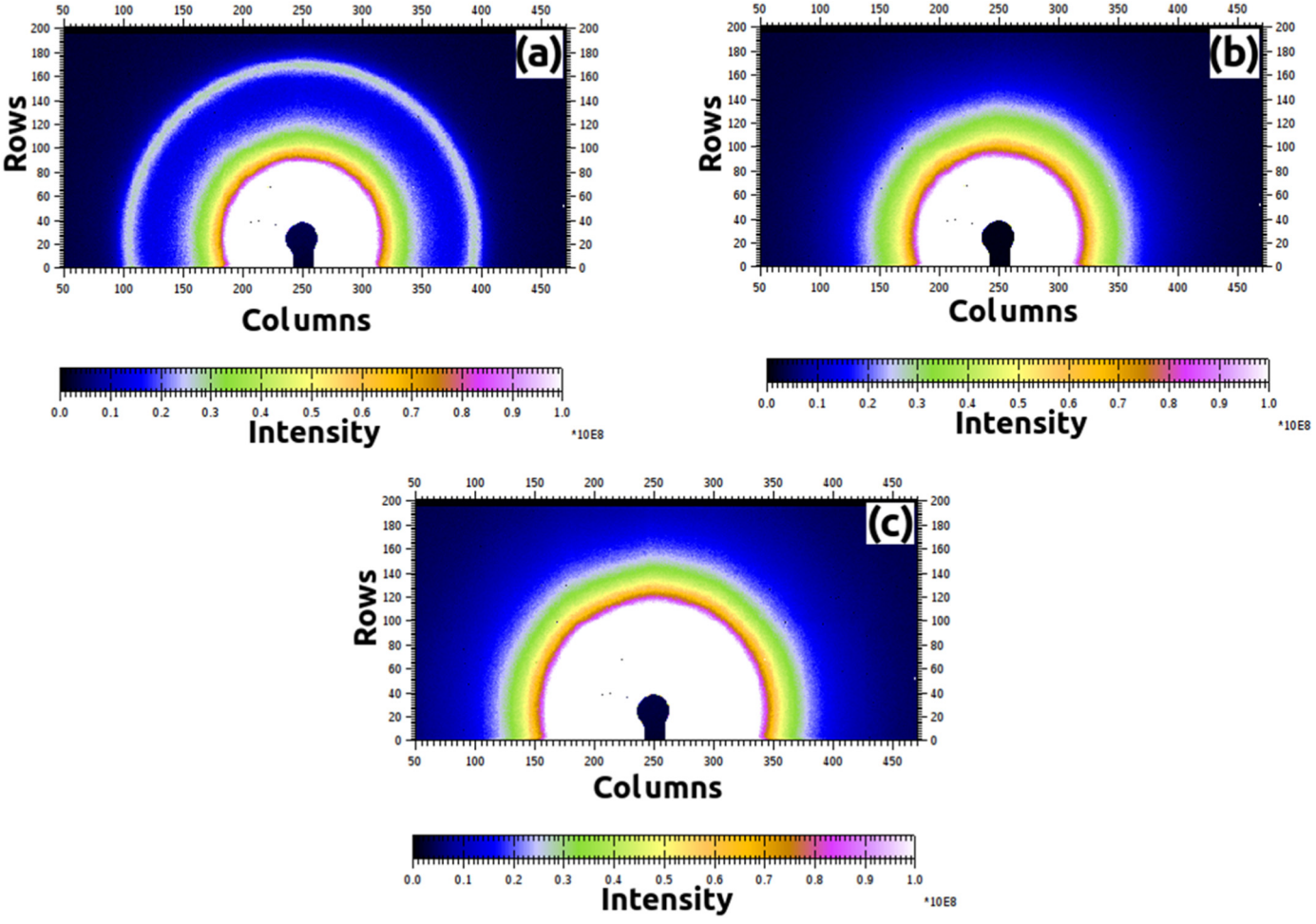

Fig. 3. Two-dimensional SAXS patterns of PBS (a), composite containing 5.0% of maghemite (b), and maghemite (c).

Table 2
SAXS data used to characterize the macro-structure of the PBS.

Peak	q (nm^{-1})	Lamellae	Hexagonal	Gyroid	BBC	CFC	Orthorhombic
1	1.138	1.138	1.138	1.138	1.138	1.138	1.138
2	2.279	2.276	1.971	1.61	1.61	1.314	2.369
3	2.764	3.414	2.276	2.788	1.971	1.859	2.545
R^2		0.9739	**0.9995**	0.8909	0.9883	0.8698	0.9839
p		0.146	**0.021**	0.300	0.098	0.329	0.114

Bold values indicate statistically significance at $p < 0.05$.

30.28°, 35.66°, 43.34°, 53.86°, 57.50° and 62.97°. These peaks correspond to the (220), (311), (400), (422), (511) and (440) crystalline planes in an orthorhombic cell of the cubic spinel structure, respectively (Marques et al., 2016; Oliveira et al., 2013). This kind of crystalline structure is characteristic of γ-Fe_2O_3-type paramagnetic particles (Péres et al., 2014).

Fig. 2 also shows the XRD pattern of PBS, composites, and maghemite. PBS presents characteristic peaks centered at 2θ values equal to 19.55°; 21.90°; 22.65°; and 28.91°. These peaks correspond to the (020), (021), (110), and (111) crystalline planes in a monoclinic cell (Papageorgiou et al., 2014).

As shown in Fig. 2, the peaks of the PBS are present in the composites, indicating that the main crystalline structure of the polymer remains similar, independently of the amount of maghemite. Only the composite filled with 5.0 wt% of maghemite presents a peak of this magnetic material, centered at 35.50°. The crystallite sizes (Lc) of pure maghemite and maghemite inside the last composite were calculated from the peak at 2θ centered at 35.66°. The average maghemite crystallite size (Lc) was (23 ± 2) nm, while the composite containing 5 wt% of maghemite presented crystallite sizes of (28 ± 3) nm. These values are statistically the same, which proves that the nanoparticles did not suffer any changes during the matrix mixture process, keeping their properties (Marques et al., 2017; Oliveira et al., 2012). Besides that, the TEM micrography, shown as the inset (#) of Fig. 2, allowed inferring that magnetic nanoparticles possess average diameter equal to (21 ± 8) nm. This result is in complete agreement with the XRD one.

In turn, despite the presence of all the PBS peaks in the composites, a deeper analysis of the XRD data (see Table 1) allowed inferring that crystallinity degree of the samples decreases with the increase of the maghemite amount. More than this, the observed decrease of the crystalline degree follows a linear behavior, with correlation equal to −0.952. This result proves that changes are taking place in the composites. Also, the analysis of the peak centered at 2θ = 22.65° demonstrates that the area of the (110) peak decreases from 1503 to 507 ($R = -0.928$). Unfortunately, further microstructural parameters could not be calculated since the correlation between FWHM and the used amount of maghemite presented $p > 0.05$.

Samples were also studied by SAXS. The two-dimensional scattering patterns (2D-SAXS) of selected samples are shown in Fig. 3.

PBS presents an anisotropic pattern, composed of clearly defined scattering events caused by the presence of organized macrostructures. (Kumar et al., 2013). On the other hand, the composite and maghemite, besides the halo effect, do not present this kind of pattern, indicating the random dispersion of these particles (Nappini et al., 2016). In turn, Fig. 4 shows the 1D-SAXS patterns of same materials.

SAXS of the PBS was deconvoluted into three peaks centered at 1.138, 2.279 and 2.764 nm^{-1}. Aiming to understand the morphology of the polymer, obtained data were compared to results that describe typical crystalline models. The tested models were: lamellae (q, 2q, 3q), hexagonal (q, $3^{1/2}$ q, $4^{1/2}$ q), gyroid (q, $(8/3)^{1/2}$ q), body centered cubic - BCC (q, $2^{1/2}$ q, $3^{1/2}$ q), face centered cubic - CFC (q, $(4/3)^{1/2}$ q,

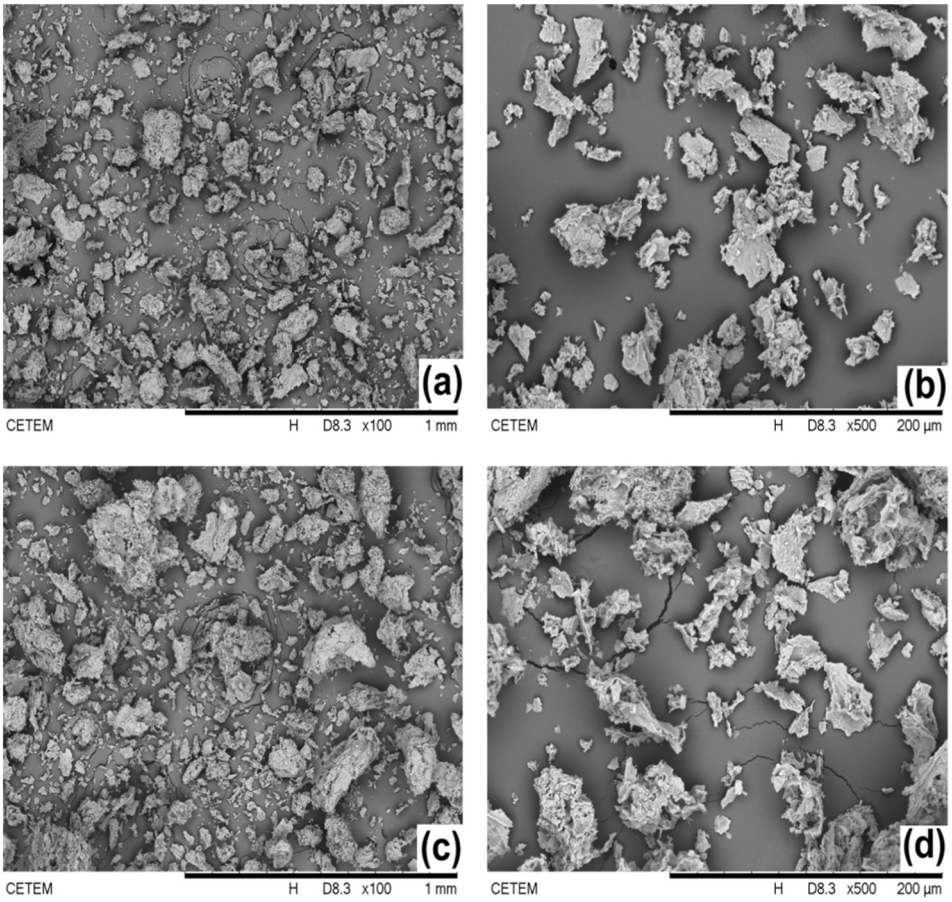

Fig. 5. SEM of PBS magnified 100× (a), PBS magnified 500× (b), composite containing 5.0% of maghemite magnified 100× (c) and 500× (d).

$(8/3)^{1/2}$ q, $(11/3)^{1/2}$ q) and orthorhombic (q, $(13/3)^{1/2}$ q, $(5)^{1/2}$ q, $(16/3)^{1/2}$ q) (Souza Jr. et al., 2008). Among them, the unique system with $p < 0.05$ was the Hexagonal, as proved in Table 2.

As demonstrated elsewhere (Souza Jr. et al., 2008), the presence of interference peaks in 1D-SAXS reveals the existence of spatial correlations between heterogeneities of nanometric scale (Glatter, 1982; Souza Jr. et al., 2007). In this case, the SAXS curve becomes similar to that corresponding to the wide angle scattering produced by disordered atomic structures. Under this assumption, an average and most probable distance d_S between heterogeneities can be estimated as:

$$D_S = 2\,\pi\,q_{max} \tag{5}$$

where q_{max} is the modulus of the scattering vector at the peak maximum. Therefore, for PBS, the peaks centered at 1.138, 2.279 and 2.764 nm^{-1} corresponds to the hexagonal planes q_{10}, q_{11}, and q_{20}, respectively. These hexagonal planes possess d_S values equal to 5.521, 2.756, and 2.273 nm, respectively.

Information about the degree of order between the heterogeneities can be obtained from the width of the SAXS peaks (Glatter, 1982; Souza Jr. et al., 2007). The average size of the correlation volume associated with the spatial distribution of heterogeneities (an estimative of the disordered "super-crystal" size), L_C, can be obtained with the Scherrer equation as:

$$L_c = \frac{4 \times \pi}{\Delta q} \tag{6}$$

where Δq is the full width at half maximum (FWHM) of the correlation peak of the SAXS function (Glatter, 1982). For PBS, the values of L_C associated to the peaks located at 1.138, 2.279 and 2.764 $nm^{-1}$are equal to 113.655 ($R^2 = 0.989$), 73.925 ($R^2 = 0.984$), and 70.627 nm ($R^2 = 0.924$), respectively. These results allowed calculating the number of

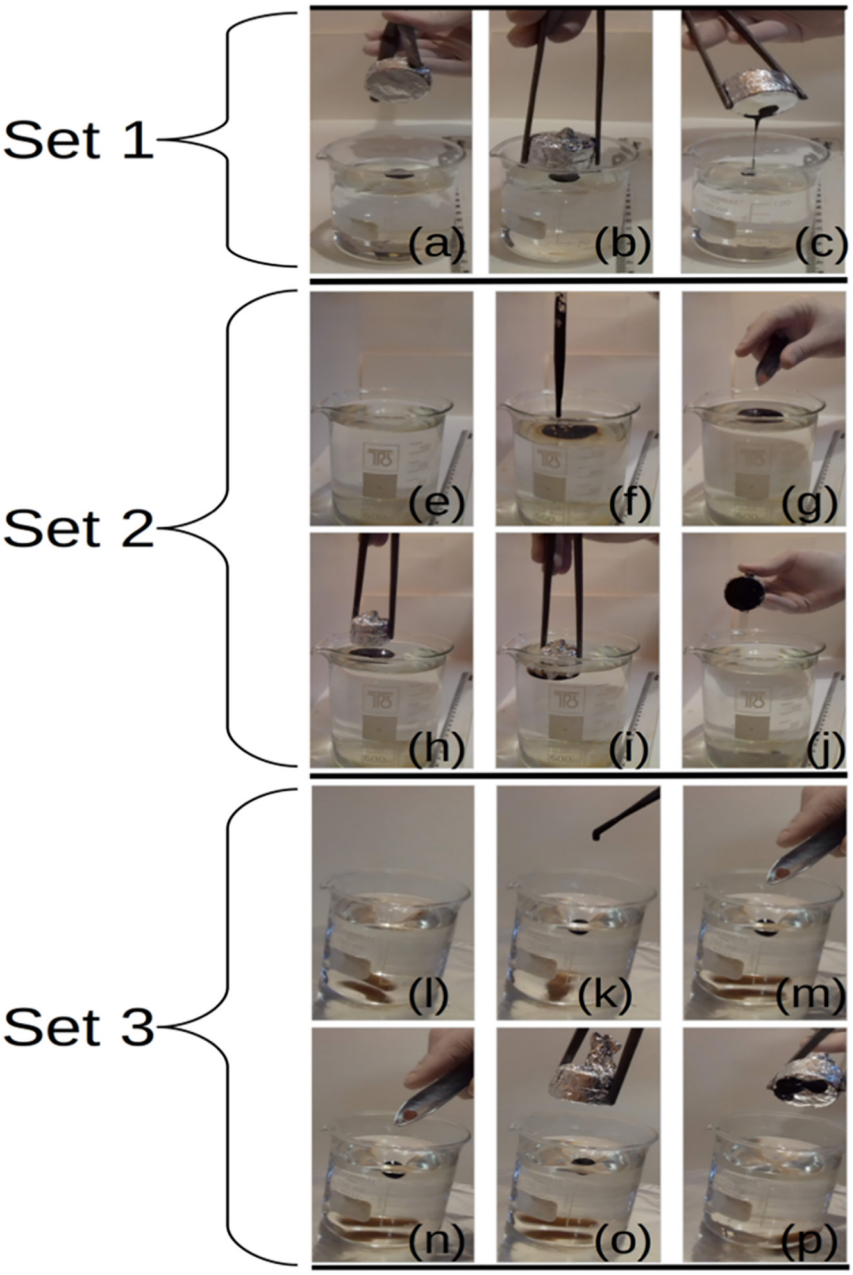

Fig. 6. Oil spill cleanup test without magnetic composite (Set 1 – *a* up to *c*), using magnetic nanocomposites without (Set 2 – *e* up to *j*) and under stirring (Set 3 – *l* up to *p*).

stacked planes, which is equal to Lc/d_S. Thus, PBS sample is composed by 21, 27, and 31 stacked plans type q_{10}, q_{11}, and q_{20}, respectively. These results are significant because they reveal the high order of PBS, which ranges from the WAXS to the SAXS region. This long structure characteristic is crucial to the oil sorbing applications since PBS here used can be considered as a physical thermoset, which will not easily dissolve in the presence of the flowing organic media.

Aiming to improve the understanding of the prepared materials, the PBS and the composite filled with 5% of magnetic nanoparticles also were studied using SEM. The obtained results are shown in Fig. 5.

PBS and composite particles presented a rough surface, which can be useful to increase the sorption of the oil. Besides that, both materials presented, with 95% of confidence, the same average diameter. Specifically, PBS and composite containing 5.0% of maghemite presented average diameters equal to (21.9 ± 3.2) μm and (19.6 ± 2.6) μm, respectively. These results allowed inferring the obtaining of products with the same granulometry.

Magnetite and maghemite were also studied using the magnetic force test. Pure magnetite and maghemite presented magnetic force equal to (488 ± 1) and (890 ± 4) mN/g, respectively. Therefore, despite some agglomeration, the use of maghemite is justified by its stronger magnetic force. Composites presented increasing magnetic force values. For instance, composites filled with 0.5, 1.5, 2.5, 3.5 and 5.0% of maghemite presented magnetic force values (@ 757 G) equal to (5.29 ± 0.06), (11.69 ± 0.16), (21.38 ± 0.61), (25.73 ± 0.64), and (61.22 ± 0.16) mN/g, respectively. As expected, the observed magnetic force increase can be linearly described as a function of maghemite amount with a correlation equal to 0.99396 ($p = 0.00056$ or 99.944% of probability). The calculated increase magnetic force rate as a function of the used amount of magnetic nanoparticles was equal to (10.2 ± 1.1) mN/g%. The same composites were also tested as sorbing materials, as illustrated in Fig. 6.

Fig. 6, Set 1 shows the interaction between the oil and the magnet. As one can see in Fig. 6(a), the oil was spilled on the brine. Then, the magnet touched the oil (see Fig. 6(b)), where it did not remain stuck (see Fig. 6(c)). Actually, after two or 3 min, all the oil was spilled again on the water.

In turn, Fig. 6, Set 2 shows the effect of the insertion of the nanocomposite filled with 5% of the magnetic nanoparticles on the oil spill removal capability without stirring. First, the oil was spilled on the brine (see Fig. 6(e) & (f)). Then, the nanocomposite was dispersed on the oil (see Fig. 6(g)). Soon afterward, the magnet was kept in touch with the organic phase (see Fig. 6(g) & (i)), from where it was able to keep all the oil stuck on its surface, as shown in Fig. 6(j).

Finally, Fig. 6, Set 3 shows the effect of the insertion of the nanocomposite filled with 5% of the magnetic nanoparticles on the oil spill removal capability under stirring. In this case, the system containing brine was kept under 75 rpm (Fig. 6(l)). Then, the oil was spilled on the brine, and the nanocomposite was dispersed on the oil (see Figs. 6 (k) to (n)). Soon afterward, the magnet was kept in touch with the organic phase (see Fig. 6(o)), from where it was able to keep all the oil stuck on its surface (see Fig. 6(p)).

The gravimetric oil removal tests were performed using a Nd magnet, and obtained results are presented as grams of the oil removed by each gram of the composite, being the results dimensionless. The composites containing 0.0, 0.5, 1.5, 2.5, 3.5, and 5.0 wt% of maghemite presented oil removal capability equal to (9.63 ± 0.46) g/g, (10.34 ± 0.74) g/g, (10.74 ± 0.20) g/g, (10.63 ± 0.35) g/g, and (11.06 ± 0.48) g/g, respectively. Therefore, in the best case, each gram of the resin can remove around 11 g of the petroleum from the water. According to the $p < 0.05$ criteria, the oil removed from the water cannot be linearly described as a function of the maghemite amount since results presented a correlation equal to 0.84064 ($p = 0.07452$ or 92.548% of probability). On the other hand, the calculated probability (92.548%)

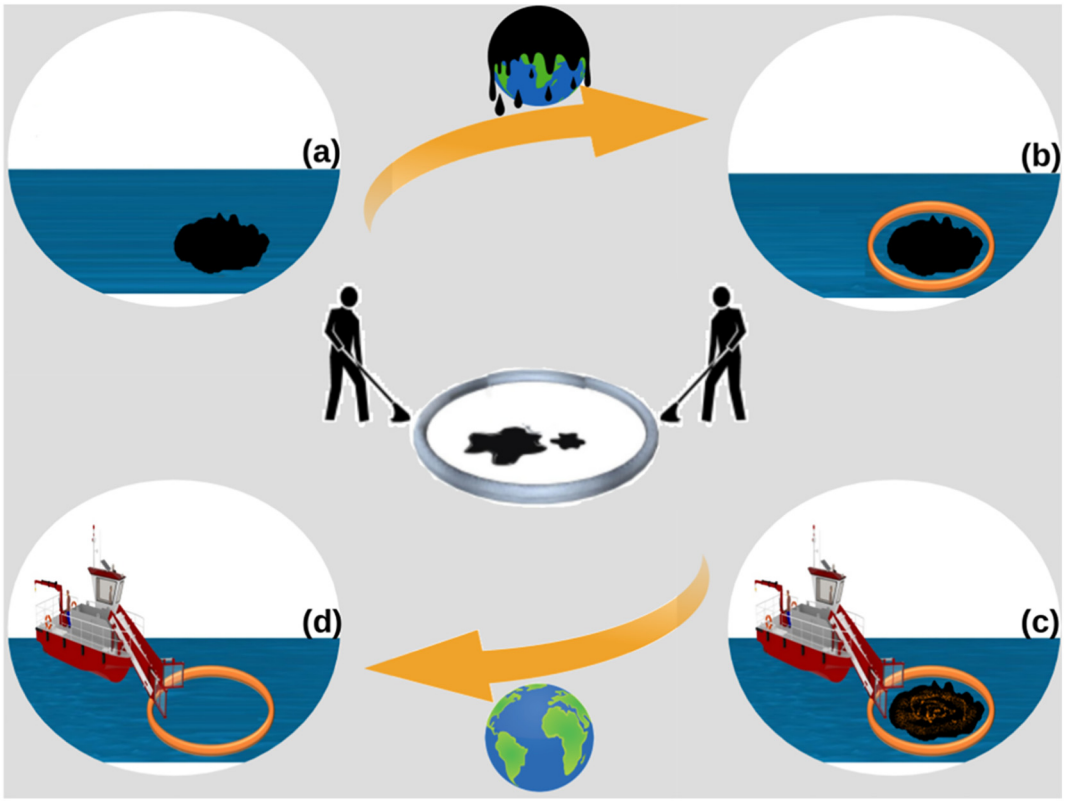

Fig. 7. Continuous oil spill cleanup process: oil spilled on the water (a), petroleum contained by skimmers (b), nanocomposite spread on the oil (c), and environment fully recovered (d).

allows us to infer that the increasing amount of magnetic nanoparticles produces an increasing tendency of the observed oil removal capability values. As demonstrated by our group elsewhere (Varela et al., 2013), these results show that the increase of the maghemite concentration inside the biocomposite increases the removal efficiency of the oil from the water. This phenomenon is due to the larger magnetic attraction between the magnetic particles and the magnet, which is responsible for the formation of a strongly bonded network. This network presents voids able to trap the petroleum. Also, this network produces a surface interaction between nanocomposite and oil associated with it. Thus, due to these two factors, the achieved network can capture and seal more and more petroleum inside itself as more and more magnetic nanoparticles are used. So, as demonstrated again, the oil removal capability is the sum of two distinct effects, related to the magnetic force and of the affinity between the bioresin and the oil. Besides, this is a very encouraging result, since as reported earlier in this paper, we already produced magnetic resins based on aliphatic/aromatic polyester matrix filled with coffee ground powder able to remove 25 g of the petroleum from the water. All these results lead us to conclude that the key to higher oil sorption capability using polyesters mainly lays on the aliphatic/aromatic balance, which can be easily achieved with slight modifications in the polyesters chains. Besides that, the used amount of magnetic nanoparticles can increase the oil removal capability of the composite as well. Therefore, the result here presented is auspicious, since PBS can be modified with natural species, as we proved using rutin (Ferreira et al., 2017), changing its aliphatic/aromatic balance and possibly improving its oil sorbing capability. We recommend this approach, and we will use it in our next works.

Finally, as shown in Fig. 7, the tested material can be useful to the continuous removal of petroleum from the water, by using belts like the ones commercially described by the MAVI DENIZ Co. (DENIZ, 2017).

This company produces coastal Anti-Pollution Vessels ® able to remove trash and oil spilled from the water. In this case, a small adaptation, allowing for the use of magnetizable belts, could grab the magnetic nanocomposites removing continuously and more efficiently the system nanocomposites/sorbed oil from the water. This conceptual automatic cleanup process can be the difference between the contaminated site and the recovery of this critical resource.

4. Conclusions

PBS, mainly due to its high crystallinity degree behaves as an insoluble material in petroleum. The melting mixing preparation did not affect the crystallinity of the tested materials neither the intrinsic properties of the nanoparticles, as demonstrated by XRD tests, allowing the development of magnetic composites able to be used as oil spill cleanup tools. In the best case, 1 g of the composite was able to remove 11 g of the petroleum from the water. This result is interesting since PBS is a platform material, which will become cheaper in the next years. Therefore, these results are encouraging and lead us to propose new studies involving PBS modified with aromatic components, which could improve the oil removal capability of this green polymer.

Acknowledgments

The authors thank Instituto Nacional de Metrologia Normalização e Qualidade Industrial (Inmetro) for the transmission electron microscope (FEI-Tecnai Spirit 12), Conselho Nacional de Desenvolvimento Científico e Tecnológico (CNPq 474940/2012-8, 550030/2013-1, and 301461/2015-5), Coordenação de Aperfeiçoamento de Pessoal de Nível Superior (CAPES), Financiadora de Estudos e Projetos (FINEP PRESAL Ref. 1889/10), Brazilian Synchrotron Light Laboratory (SAXS1-20160027) and Fundação Carlos Chagas Filho de Amparo à Pesquisa do Estado do Rio de Janeiro (FAPERJ) for the financial support and scholarships.

Declarations of interest

None.

References

A repeated sampling method for oil spill impact uncertainty and interpolation, 2017. Int. J. Disaster Risk Reduct. 22, 420–430. https://doi.org/10.1016/j.ijdrr.2017.01.014.

Adebajo, M.O., Frost, R.L., Kloprogge, J.T., Carmody, O., Kokot, S., 2003. Porous Materials for oil spill cleanup: a review of synthesis and absorbing properties. J. Porous Mater. 10, 159–170. https://doi.org/10.1023/A:1027484117065.

Avila, A.F., Munhoz, V.C., de Oliveira, A.M., Santos, M.C.G., Lacerda, G.R.B.S., Gonçalves, C.P., 2014. Nano-based systems for oil spills control and cleanup. J. Hazard. Mater. 272, 20–27. https://doi.org/10.1016/j.jhazmat.2014.02.038.

Bourmaud, A., Corre, Y.-M., Baley, C., 2015. Fully biodegradable composites: use of poly-(butylene-succinate) as a matrix and to plasticize l-poly-(lactide)-flax blends. Ind. Crop. Prod. 64, 251–257. https://doi.org/10.1016/j.indcrop.2014.09.033.

Carroll, J., Vikebø, F., Howell, D., Broch, O.J., Nepstad, R., Augustine, S., Skeie, G.M., Bast, R., Juselius, J., 2018. Assessing impacts of simulated oil spills on the Northeast Arctic cod fishery. Mar. Pollut. Bull. 126, 63–73. https://doi.org/10.1016/j.marpolbul.2017.10.069.

Charlier, Q., Girard, E., Freyermouth, F., Vandesteene, M., Jacquel, N., Ladaviere, C., Rousseau, A., Fenouillot, F., 2015. Solution viscosity–molar mass relationships for poly(butylene succinate) and discussion on molar mass analysis. Express Polym Lett 9.

Cheng, K.-K., Zhao, X.-B., Zeng, J., Zhang, J.-A., 2012. Biotechnological production of succinic acid: current state and perspectives. Biofuels, Bioprod. Biorefin. 6, 302–318. https://doi.org/10.1002/bbb.1327.

Clancy, S.A., Worrall, F., Davies, R.J., Gluyas, J.G., 2018. The potential for spills and leaks of contaminated liquids from shale gas developments. Sci. Total Environ. https://doi.org/10.1016/j.scitotenv.2018.01.177.

Cohen, J., Cohen, P., 1983. Applied Multiple Regression/Correlation Analysis for the Behavioral Sciences. Taylor & Francis.

da Costa, R.C., Souza Jr., F.G., 2014. Preparo de nanocompósitos de maghemita e polianilina assistido por ultrassom. Polímeros 24, 243–249. https://doi.org/10.4322/polimeros.2014.035.

DENIZ, M., 2017. MAVI DENIZ Subcontracted Coastal 3× OSRV + 1× Pollution Control Boat. MAVIDENIZ.

Di Lorenzo, M.L., Androsch, R., Righetti, M.C., 2017. Low-temperature crystallization of poly(butylene succinate). Eur. Polym. J. 94, 384–391. https://doi.org/10.1016/j.eurpolymj.2017.07.025.

Doshi, B., Sillanpää, M., Kalliola, S., 2018a. A review of bio-based materials for oil spill treatment. Water Res. https://doi.org/10.1016/j.watres.2018.02.034.

Doshi, B., Repo, E., Heiskanen, J.P., Sirviö, J.A., Sillanpää, M., 2018b. Sodium salt of oleoyl carboxymethyl chitosan: a sustainable adsorbent in the oil spill treatment. J. Cleaner Prod. 170, 339–350. https://doi.org/10.1016/j.jclepro.2017.09.163.

Duan, J., Liu, W., Zhao, X., Han, Y., O'Reilly, S.E., Zhao, D., 2018. Study of residual oil in Bay Jimmy sediment 5 years after the Deepwater Horizon oil spill: Persistence of sediment retained oil hydrocarbons and effect of dispersants on desorption. Sci. Total Environ. 618, 1244–1253. https://doi.org/10.1016/j.scitotenv.2017.09.234.

Ferreira, L.P., Moreira, A.N., Delazare, T., Oliveira, G.E., Souza Jr., F.G., 2012. Petroleum absorbers based on CNSL, furfural and lignin – the effect of the chemical similarity on the interactions among petroleum and bioresins. Macromol. Symp. 319, 210–221. https://doi.org/10.1002/masy.201100145.

Ferreira, L.P., da Cunha, B.P., Kuster, R.M., Pinto, J.C., Souza, M.N., Souza Jr., F.G., 2017. Synthesis and chemical modification of poly(butylene succinate) with rutin useful to the release of silybin. Ind. Crop. Prod. 97, 599–611. https://doi.org/10.1016/j.indcrop.2016.12.064.

Frollini, E., Bartolucci, N., Sisti, L., Celli, A., 2013. Poly(butylene succinate) reinforced with different lignocellulosic fibers. Ind. Crop. Prod. 45, 160–169. https://doi.org/10.1016/j.indcrop.2012.12.013.

Giari, L., Dezfuli, B.S., Lanzoni, M., Castaldelli, G., 2012. The impact of an oil spill on organs of bream *Abramis brama* in the Po River. Ecotoxicol. Environ. Saf. 77, 18–27. https://doi.org/10.1016/j.ecoenv.2011.10.014.

Gigli, M., Fabbri, M., Lotti, N., Gamberini, R., Rimini, B., Munari, A., 2016. Poly(butylene succinate)-based polyesters for biomedical applications: a review. Eur. Polym. J. 75, 431–460.

Glatter, O., 1982. Small Angle X-ray Scattering. Academic Press.

Grance, E.G.O., Souza Jr., F.G., Varela, A., Pereira, E.D., Oliveira, G.E., Rodrigues, C.H.M., 2012. New petroleum absorbers based on lignin-CNSL-formol magnetic nanocomposites. J. Appl. Polym. Sci. 126, E305–E312. https://doi.org/10.1002/app.36998.

Gu, J., Jiang, W., Wang, F., Chen, M., Mao, J., Xie, T., 2014. Facile removal of oils from water surfaces through highly hydrophobic and magnetic polymer nanocomposites. Appl. Surf. Sci. 301, 492–499. https://doi.org/10.1016/j.apsusc.2014.02.112.

Gunster, D.G., Bonnevie, N.L., Gillis, C.A., Wenning, R.J., 1993. Assessment of chemical loadings to Newark Bay, New Jersey from petroleum and hazardous chemical accidents occurring from 1986 to 1991. Ecotoxicol. Environ. Saf. 25, 202–213. https://doi.org/10.1006/eesa.1993.1019.

Heibati, B., Pollitt, K.J.G., Karimi, A., Yazdani Charati, J., Ducatman, A., Shokrzadeh, M., Mohammadyan, M., 2017. BTEX exposure assessment and quantitative risk assessment among petroleum product distributors. Ecotoxicol. Environ. Saf. 144, 445–449. https://doi.org/10.1016/j.ecoenv.2017.06.055.

Ismail, Z., Karim, R., 2013. Some technical aspects of spills in the transportation of petroleum materials by tankers. Saf. Sci. 51, 202–208. https://doi.org/10.1016/j.ssci.2012.06.024.

Kaiser, M.J., Liu, M., 2018. A scenario-based deepwater decommissioning forecast in the U.S. Gulf of Mexico. J. Pet. Sci. Eng. https://doi.org/10.1016/j.petrol.2018.01.073.

Kelley, K., Lai, K., 2011. Accuracy in parameter estimation for the root mean square error of approximation: sample size planning for narrow confidence intervals. Multivar. Behav. Res. 46, 1–32. https://doi.org/10.1080/00273171.2011.543027.

Kennouche, S., Le Moigne, N., Kaci, M., Quantin, J.-C., Caro-Bretelle, A.-S., Delaite, C., Lopez-Cuesta, J.-M., 2016. Morphological characterization and thermal properties of compatibilized poly(3-hydroxybutyrate-co-3-hydroxyvalerate) (PHBV)/poly(butylene succinate) (PBS)/halloysite ternary nanocomposites. Eur. Polym. J. 75, 142–162. https://doi.org/10.1016/j.eurpolymj.2015.12.009.

Klavins, M., Porshnov, D., Ansone, L., Robalds, A., Dreijalte, L., 2012. Peat as natural and industrial sorbent. Recent Res. Environ. Energy Syst. Sustain. 2, 146–162.

Kumar, R., Sides, S.W., Goswami, M., Sumpter, B.G., Hong, K., Wu, X., Russell, T.P., Gido, S.P., Misichronis, K., Rangou, S., Avgeropoulos, A., Tsoukatos, T., Hadjichristidis, N., Beyer, F.L., Mays, J.W., 2013. Morphologies of ABC triblock terpolymer melts containing poly(cyclohexadiene): effects of conformational asymmetry. Langmuir 29, 1995–2006. https://doi.org/10.1021/la304576c.

Li, Q., Yang, M., Wang, D., Li, W., Wu, Y., Zhang, Y., Xing, J., Su, Z., 2010. Efficient conversion of crop stalk wastes into succinic acid production by *Actinobacillus succinogenes*. Bioresour. Technol. 101, 3292–3294. https://doi.org/10.1016/j.biortech.2009.12.064.

Li, H., Liu, L., Yang, F., 2012. Hydrophobic modification of polyurethane foam for oil spill cleanup. Mar. Pollut. Bull. 64, 1648–1653. https://doi.org/10.1016/j.marpolbul.2012.05.039.

Li, Y., Zhang, J., Cheng, P., Shi, J., Yao, L., Qiu, Y., 2014. Helium plasma treatment voltage effect on adhesion of ramie fibers to polybutylene succinate. Ind. Crop. Prod. 61, 16–22. https://doi.org/10.1016/j.indcrop.2014.06.039.

Lin, J., Shang, Y., Ding, B., Yang, J., Yu, J., Al-Deyab, S.S., 2012. Nanoporous polystyrene fibers for oil spill cleanup. Mar. Pollut. Bull. 64, 347–352. https://doi.org/10.1016/j.marpolbul.2011.11.002.

Liu, Y., Li, X., Hu, P., Hu, G., 2015. Study on the supercooling degree and nucleation behavior of water-based graphene oxide nanofluids PCM. Int. J. Refrig 50, 80–86. https://doi.org/10.1016/j.ijrefrig.2014.10.019.

Lobakova, E., Vasilieva, S., Kashcheeva, P., Ivanova, E., Dolnikova, G., Chekanov, K., Idiatulov, R., Kirpichnikov, M., Buznik, V., Dedov, A., 2016. New bio-hybrid materials for bioremoval of crude oil spills from marine waters. Int. Biodeterior. Biodegrad. 108, 99–107. https://doi.org/10.1016/j.ibiod.2015.12.016.

Lopes, M.C., Souza Jr., F.G., Oliveira, G.E., 2010. Espumados magnetizáveis úteis em processos de recuperação ambiental. Polímeros 20, 359–365. https://doi.org/10.1590/S0104-14282010005000054.

Luzi, F., Fortunati, E., Jiménez, A., Puglia, D., Pezzolla, D., Gigliotti, G., Kenny, J.M., Chiralt, A., Torre, L., 2016. Production and characterization of PLA_PBS biodegradable blends reinforced with cellulose nanocrystals extracted from hemp fibres. Ind. Crops Prod, Nanocellulose: Production, Functionalisation and Applications. 93, pp. 276–289. https://doi.org/10.1016/j.indcrop.2016.01.045.

Marques, F.D., Souza Jr., F.G., Oliveira, G.E., 2016. Oil sorbers based on renewable sources and coffee grounds. J. Appl. Polym. Sci. 133, 43127–43134. https://doi.org/10.1002/app.43127.

Marques, F.D., Nele De Souza, M., Souza Jr., F.G., 2017. Sealing system activated by magnetic induction polymerization. J. Appl. Polym. Sci. 134, 45549. https://doi.org/10.1002/app.45549.

Medeiros, L.C.C., Delunardo, F.A.C., Simões, L.N., Paulino, M.G., Vargas, T.S., Fernandes, M.N., Scherer, R., Chippari-Gomes, A.R., 2017. Water-soluble fraction of petroleum induces genotoxicity and morphological effects in fat snook (*Centropomus parallelus*). Ecotoxicol. Environ. Saf. 144, 275–282. https://doi.org/10.1016/j.ecoenv.2017.06.031.

Messina, E., Denaro, R., Crisafi, F., Smedile, F., Cappello, S., Genovese, M., Genovese, L., Giuliano, L., Russo, D., Ferrer, M., Golyshin, P., Yakimov, M.M., 2016. Genome sequence of obligate marine polycyclic aromatic hydrocarbons-degrading bacterium *Cycloclasticus* sp. 78-ME, isolated from petroleum deposits of the sunken tanker Amoco Milford Haven, Mediterranean Sea. Mar. Genomics 25, 11–13. https://doi.org/10.1016/j.margen.2015.10.006.

Motta, F.L., Stoyanov, S.R., Soares, J.B.P., 2018. Application of solidifiers for oil spill containment: a review. Chemosphere 194, 837–846. https://doi.org/10.1016/j.chemosphere.2017.11.103.

Murphy, D., Gemmell, B., Vaccari, L., Li, C., Bacosa, H., Evans, M., Gemmell, C., Harvey, T., Jalali, M., Niepa, T.H.R., 2016. An in-depth survey of the oil spill literature since 1968: long term trends and changes since Deepwater Horizon. Mar. Pollut. Bull. 113, 371–379. https://doi.org/10.1016/j.marpolbul.2016.10.028.

Nappini, S., Fogli, S., Castroflorio, B., Bonini, M., Bombelli, F.B., Baglioni, P., 2016. Magnetic field responsive drug release from magnetoliposomes in biological fluids. J. Mater. Chem. B 4, 716–725. https://doi.org/10.1039/C5TB02191J.

Nerantzaki, M., Filippousi, M., Van Tendeloo, G., Terzopoulou, Z., Bikiaris, D., Goudouri, O.M., Detsch, R., Grüenewald, A., Boccaccini, A.R., 2015. Novel poly(butylene succinate) nanocomposites containing strontium hydroxyapatite nanorods with enhanced osteoconductivity for tissue engineering applications. Express Polym. Lett. 9.

Neves, J.S., Souza Jr., F.G., Suarez, P.A.Z., Umpierre, A.P., Machado, F., 2011. In situ production of polystyrene magnetic nanocomposites through a batch suspension polymerization process. Macromol. Mater. Eng. 296, 1107–1118. https://doi.org/10.1002/mame.201100050.

Nghiem, N.P., Hicks, K.B., Johnston, D.B., 2010. Integration of succinic acid and ethanol production with potential application in a corn or barley biorefinery. Appl. Biochem. Biotechnol. 162, 1915–1928. https://doi.org/10.1007/s12010-010-8969-1.

Oliveira, G.E., Souza Jr., F.G., Lopes, M.C., 2012. Magnetic biofoams based on polyurethane applied in oil spill cleanup processes - chapter 23. Natural Polymers, Biopolymers, Biomaterials, and Their Composites, Blends, and IPNs - CRC Press Book. Apple Academic Press, Inc., 1613 Beaver Dam Road, Suite 104 Point Pleasant, NJ 08742 USA, p. 370.

Oliveira, G.E., Clarindo, J.E.S., Santo, K.S.E., Souza Jr., F.G., 2013. Chemical modification of cobalt ferrite nanoparticles with possible application as asphaltene flocculant agent. Mater. Res. 0–0. https://doi.org/10.1590/S1516-14392013005000048.

Papageorgiou, G.Z., Papageorgiou, D.G., Chrissafis, K., Bikiaris, D., Will, J., Hoppe, A., Roether, J.A., Boccaccini, A.R., 2014. Crystallization and melting behavior of poly(butylene succinate) nanocomposites containing silica-nanotubes and strontium hydroxyapatite nanorods. Ind. Eng. Chem. Res. 53, 678–692. https://doi.org/10.1021/ie403238u.

Pereira, E.D., Souza, F.G., Santana, C.I., Soares, D.Q., Lemos, A.S., Menezes, L.R., 2013. Influence of magnetic field on the dissolution profile of cotrimoxazole inserted into poly (lactic acid-co-glycolic acid) and maghemite nanocomposites. Polym. Eng. Sci. 53, 2308–2317. https://doi.org/10.1002/pen.23606.

Pereira, E.D., Souza Jr., F.G., Pinto, J.C.C.S., Cerruti, R., Santana, C., 2014. Synthesis, characterization and drug delivery profile of magnetic PLGA-PEG-PLGA/maghemite nanocomposite. Macromol. Symp. 343, 18–25. https://doi.org/10.1002/masy.201300168.

Péres, E.U.X., Souza Jr., F.G., Silva, F.M., Chaker, J.A., Suarez, P.A.Z., 2014. Biopolyester from ricinoleic acid: synthesis, characterization and its use as biopolymeric matrix for magnetic nanocomposites. Ind. Crop. Prod. 59, 260–267. https://doi.org/10.1016/j.indcrop.2014.05.031.

Phua, Y.J., Chow, W.S., Mohd Ishak, Z.A., 2013. Reactive processing of maleic anhydride-grafted poly(butylene succinate) and the compatibilizing effect on poly(butylene succinate) nanocomposites. Express Polym. Lett. 7.

Rabalais, N.N., Smith, L.M., Turner, R.E., 2018. The Deepwater Horizon oil spill and Gulf of Mexico shelf hypoxia. Cont. Shelf Res. 152, 98–107. https://doi.org/10.1016/j.csr.2017.11.007.

Raj, K.G., Joy, P.A., 2015. Coconut shell based activated carbon–iron oxide magnetic nanocomposite for fast and efficient removal of oil spills. J. Environ. Chem. Eng. 3, 2068–2075. https://doi.org/10.1016/j.jece.2015.04.028.

Reynolds, John G., Paul, L.W.H., Coronado, R., 2001. Hydrophobic aerogels for oil-spill cleanup? Intrinsic absorbing properties. Energy Sources, Part A 23, 831–843. https://doi.org/10.1080/009083101316931906.

Roca, A.G., Marco, J.F., del Puerto Morales, M., Serna, C.J., 2007. Effect of nature and particle size on properties of uniform magnetite and maghemite nanoparticles. J. Phys. Chem. C 111, 18577–18584. https://doi.org/10.1021/jp075133m.

Ruland, W., 1961. X-ray determination of crystallinity and diffuse disorder scattering. Acta Crystallogr. 14, 1180–1185. https://doi.org/10.1107/S0365110X61003429.

Scherrer, P., 1918. Bestimmung der Größe und der inneren Struktur von Kolloidteilchen mittels Röntgenstrahlen. Nachrichten Von Ges. Wiss. Zu Gött. Math.-Phys. Kl., 98–100 https://doi.org/10.1007/978-3-662-33915-2_7.

Schwertmann, U., Cornell, R.M., 2008. Iron Oxides in the Laboratory. John Wiley & Sons.

Silva, M.F., Hechenleitner, A.A.W., Irache, J.M., de Oliveira, A.J.A., Pineda, E.A.G., Silva, M.F., Hechenleitner, A.A.W., Irache, J.M., de Oliveira, A.J.A., Pineda, E.A.G., 2015. Study of thermal degradation of PLGA, PLGA nanospheres and PLGA/maghemite superparamagnetic nanospheres. Mater. Res. 18, 1400–1406. https://doi.org/10.1590/1516-1439.045415.

Silverstein, R.M., Webster, F.X., Kiemle, D.J., 2005. Spectrometric Identification of Organic Compounds. John Wiley & Sons.

Souza Jr., F.G., Ferreira, A.C., Varela, A., Oliveira, G.E., Machado, F., Pereira, E.D., Fernandes, E., Pinto, J.C., Nele, M., 2013. Methodology for determination of magnetic force of polymeric nanocomposites. Polym. Test. 32, 1466–1471. https://doi.org/10.1016/j.polymertesting.2013.09.018.

Souza Jr., F.G., Soares, B.G., Pinto, J.C., 2006. SBS/polyaniline or carbon black system: finding the optimal process and molding temperatures through experimental design. Macromol. Mater. Eng. 291, 463–469. https://doi.org/10.1002/mame.200500406.

Souza Jr., F.G., Soares, B.G., Dahmouche, K., 2007. Effect of preparation method on nanoscopic structure of conductive SBS/PANI blends: study using small-angle X-ray scattering. J. Polym. Sci. Part B Polym. Phys. 45, 3069–3077. https://doi.org/10.1002/polb.21305.

Souza Jr., F.G., Richa, P., de Siervo, A., Oliveira, G.E., Rodrigues, C.H.M., Nele, M., Pinto, J.C., 2008. New in situ blends of polyaniline and cardanol bio-resins. Macromol. Mater. Eng. 293, 675–683. https://doi.org/10.1002/mame.200800077.

Souza Jr., F.G., Marins, J., Pinto, J., de Oliveira, G., Rodrigues, C., Lima, L., 2010a. Magnetic field sensor based on a maghemite/polyaniline hybrid material. J. Mater. Sci. 45, 5012–5021. https://doi.org/10.1007/s10853-010-4321-y.

Souza Jr., F.G., Marins, J.A., Rodrigues, C.H.M., Pinto, J.C., 2010b. A magnetic composite for cleaning of oil spills on water. Macromol. Mater. Eng. 295, 942–948. https://doi.org/10.1002/mame.201000090.

Souza Jr., F.G., Ferreira, A.C., Varela, A., Oliveira, G.E., Machado, F., Pereira, E.D., Fernandes, E., Pinto, J.C., Nele, M., 2013. Methodology for determination of magnetic force of polymeric nanocomposites. Polym. Test. 32, 1466–1471. https://doi.org/10.1016/j.polymertesting.2013.09.018.

Su, C., Yang, H., Song, S., Lu, B., Chen, R., 2017. A magnetic superhydrophilic/oleophobic sponge for continuous oil-water separation. Chem. Eng. J. 309, 366–373. https://doi.org/10.1016/j.cej.2016.10.082.

U.S. Energy Information Administration, 2018. International Energy Statistics [WWW Document]. URL. https://www.eia.gov/beta/international/data/browser/#/?pa=0000000000000000000000000000000000g&c=ruvvvvvfvtvnvv1vrvvvvfvvvvvvfvvvou20evvvvvvvvvvvvvuvo&ct=0&tl_id=5-A&vs=INTL.53-1-AFG-TBPD.A&vo=0&v=H&start=2006&end=2016 (accessed 2.16.18).

Varela, A., Oliveira, G., Souza Jr., F.G., Rodrigues, C.H.M., Costa, M.A.S., 2013. New petroleum absorbers based on cardanol-furfuraldehyde magnetic nanocomposites. Polym. Eng. Sci. 53, 44–51. https://doi.org/10.1002/pen.23229.

Wang, X.-S., Liu, J., Bonefont, J.M., Yuan, D.-Q., Thallapally, P.K., Ma, S., 2013. A porous covalent porphyrin framework with exceptional uptake capacity of saturated hydrocarbons for oil spill cleanup. Chem. Commun. 49, 1533–1535. https://doi.org/10.1039/C2CC38067F.

Wang, J., Geng, G., Liu, X., Han, F., Xu, J., 2016. Magnetically superhydrophobic kapok fiber for selective sorption and continuous separation of oil from water. Chem. Eng. Res. Des. 115, 122–130. https://doi.org/10.1016/j.cherd.2016.09.032.

Wilton, N., Lyon-Marion, B.A., Kamath, R., McVey, K., Pennell, K.D., Robbat, A., 2018. Remediation of heavy hydrocarbon impacted soil using biopolymer and polystyrene foam beads. J. Hazard. Mater. 349, 153–159. https://doi.org/10.1016/j.jhazmat.2018.01.041.

Wise, J.P., Wise, J.T.F., Wise, C.F., Wise, S.S., Gianios, C., Xie, H., Walter, R., Boswell, M., Zhu, C., Zheng, T., Perkins, C., Wise, J.P., 2018. A three year study of metal levels in skin biopsies of whales in the Gulf of Mexico after the Deepwater Horizon oil crisis. Comp. Biochem. Physiol., Part C: Toxicol. Pharmacol. 205, 15–25. https://doi.org/10.1016/j.cbpc.2017.12.003.

Xu, J., Guo, B.-H., 2010. Poly(butylene succinate) and its copolymers: Research, development and industrialization. Biotechnol. J. 5, 1149–1163. https://doi.org/10.1002/biot.201000136.

Zhu, H., Qiu, S., Jiang, W., Wu, D., Zhang, C., 2011. Evaluation of electrospun polyvinyl chloride/polystyrene fibers as sorbent materials for oil spill cleanup. Environ. Sci. Technol. 45, 4527–4531. https://doi.org/10.1021/es2002343.